REPORT DOCUMENTATION PAGE

Form Approved
OMB No. 0704-0188

1. REPORT DATE *(DD-MM-YYYY)*	2. REPORT TYPE	3. DATES COVERED *(From - To)*
19/07/11	Final	02/08-02/11

4. TITLE AND SUBTITLE
Epitaxial Nucleation on Rationally Designed Peptide Functionalized Interface

5a. CONTRACT NUMBER
FA9550-08-1-0041

5b. GRANT NUMBER

5c. PROGRAM ELEMENT NUMBER

6. AUTHOR(S)
Raymond Tu

5d. PROJECT NUMBER

5e. TASK NUMBER

5f. WORK UNIT NUMBER

7. PERFORMING ORGANIZATION NAME(S) AND ADDRESS(ES)
The City College of New York - CUNY

8. PERFORMING ORGANIZATION REPORT NUMBER

9. SPONSORING/MONITORING AGENCY NAME(S) AND ADDRESS(ES)
RF CUNY

10. SPONSOR/MONITOR'S ACRONYM(S)

11. SPONSORING/MONITORING AGENCY REPORT NUMBER
AFRL-OSR-VA-TR-2012-0205

12. DISTRIBUTION AVAILABILITY STATEMENT
A

13. SUPPLEMENTARY NOTES

14. ABSTRACT

Over the course of the grant period we have applied a set of rationally designed interfacially confined peptides to explore the cooperative relationship between self-assembly and hybrid materials processing. This research report highlights our ability to apply the dynamics of surface active peptides to simultaneously control structure at two length scales, (1) the length scale associated with a fibrous peptide supramolecular assembly and (2) the length scale associated with a nucleating nano-crystalline structure. To understand the supramolecular assembly of interfacially confined peptides, we have designed a set of four amphiphilic β-sheet forming peptides and explored the role of electrostatics on phase behavior. We characterize the phase behavior by using Langmuir techniques, Brewster Angle Microscopy, Attenuated Total Reflection Fourier Transform Infrared Spectroscopy, and circular dichroism spectroscopy. We find that peptides with an alternating binary sequence transition at high pressures from discrete circular domains to fibrous domains. The qualitative behavior is independent of surface pressure but dependent on molecular areas. In addition, thermodynamic models are employed to specifically quantify differences in electrostatics by obtaining parameters for the critical aggregation area, limiting molecular area, and the dimensionless ratio of line tension to dipole density. Using these parameters, we are able to relate localized charge distribution to phase transitions. Additionally, Histidine-containing peptides are designed to examine the nucleation and growth of gold nanocrystals to the interface as a function of surface pressure. We show that peptides at low surface pressure yield large single crystalline gold domains, whereas peptides at high surface pressures yield much smaller polycrystalline gold domains. Our hypothesis states that intermediate pressures will lead to more complex structures, where the two time-scales of assembly and nucleation are similar. At intermediate pressures, the inorganic gold structures exhibit two length scales, where large single crystalline

INSTRUCTIONS FOR COMPLETING SF 298

domains appear to be connected along the self-assembling fibrous peptide template. We believe that the combination of two pathways allows us to explore a new route for materials synthesis where the dynamics of self-assembly can be directly coupled to nucleation and growth processes.

15. SUBJECT TERMS

16. SECURITY CLASSIFICATION OF:			**17. LIMITATION OF ABSTRACT**	**18. NUMBER OF PAGES**	**19a. NAME OF RESPONSIBLE PERSON**
a. REPORT	**b. ABSTRACT**	**c. THIS PAGE**			**19b. TELEPONE NUMBER (*Include area code)***

Abstract

Over the course of the grant period, we have applied a set of rationally designed interfacially confined peptides to explore the cooperative relationship between self-assembly and hybrid materials processing. This research report highlights our ability to apply the dynamics of surface active peptides to simultaneously control structure at two length scales, (1) the length scale associated with a fibrous peptide supramolecular assembly and (2) the length scale associated with a nucleating nano-crystalline structure. To understand the supramolecular assembly of interfacially confined peptides, we have designed a set of four amphiphilic β-sheet forming peptides and explored the role of electrostatics on phase behavior. We characterize the phase behavior by using Langmuir techniques, Brewster Angle Microscopy, Attenuated Total Reflection Fourier Transform Infrared Spectroscopy, and circular dichroism spectroscopy. We find that peptides with an alternating binary sequence transition from discrete circular domains to fibrous domains with increasing surface pressure. The qualitative behavior for each of the four peptides is independent of surface pressure but dependent on molecular areas. In addition, thermodynamic models are employed to specifically quantify differences in electrostatics by obtaining parameters for the critical aggregation area, limiting molecular area, and the dimensionless ratio of line tension to dipole density. Using these parameters, we are able to relate localized charge distribution to phase transitions. Additionally, Histidine-containing peptides are designed to examine the nucleation and growth of gold nanocrystals to the interface as a function of surface pressure. We show that peptides at low surface pressure yield large single crystalline gold domains, whereas peptides at high surface pressures yield much smaller polycrystalline gold domains. Our hypothesis states that intermediate pressures will lead to more complex structures, where the two time-scales of assembly and nucleation are similar. At intermediate pressures, the inorganic gold structures do indeed exhibit two length scales, where large single crystalline domains appear to be connected along the self-assembling fibrous peptide template. We believe that the combination of two pathways will allow us to explore a new route for materials synthesis.

1. Objectives

The research objective throughout the grant period has centered on the application of rationally designed peptides with two key functions: (1) the ability to self-assemble at the air-water interface and (2) the ability to control inorganic nucleation and growth processes. Our motivation for this work stems from biological systems that are capable of directing the synthesis of hierarchically structured inorganic materials, where a protein-based template can couple nucleation length scales with the length scales inherent in self-assembly processes.

Several authors have used synthetic tools to define single domain inorganic nanostructured materials. **Figure 1a** shows a single-crystal silver 'prism' that can be grown using a photo-mediated growth mechanism. [1] In contrast, biology has the ability to coordinate these discreet crystals to form a more complex functional material. The well-cited stacked-brick structure of abalone shell exemplifies how structural complexity and function are connected together, but mimicking the biological processes associated with synthesizing these complex materials remains difficult. **Figure 1b** shows another example from Lichtenegger et al, where a fibrillar copper nanostructure is generated from an organic template. The figure highlights the ability for biological molecules to control the crystalline phase of copper (atacamite) as well as the meso-scale structure to yield unique materials properties, namely, abrasion resistance.[2] Several other authors have described nature's exceptional ability to template the nucleation and growth of inorganic materials from organic precursors to generate complex materials.[2-13] Moreover, a variety of groups have used biologically inspired molecules to engineer materials from inorganic components that are not native to living organisms, including, silver[14,15], gold[14,16], Titanium[17], Co_3O_4[18], uranium oxo-species[19], GaAs[20], and ZnS[21,22].

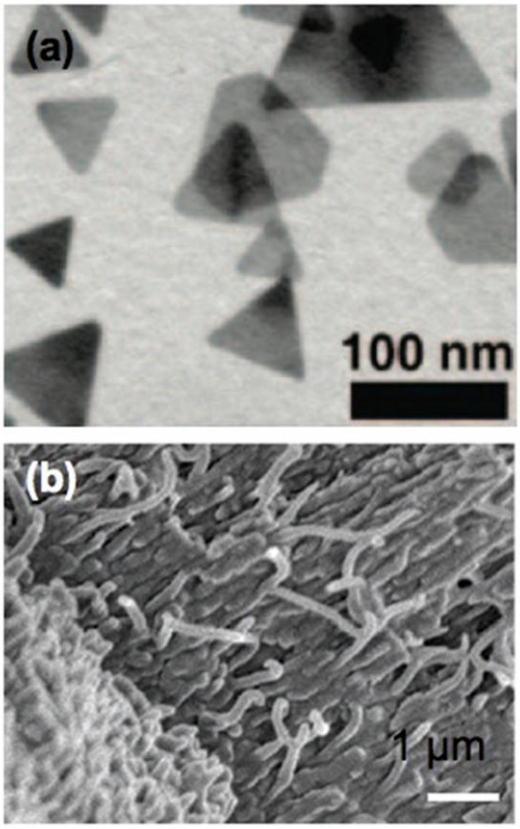

Figure 1. (a) 'Simple' synthetic silver nano-prism.[1] (b) 'Complex' biologically mediated formation of an abrasion resistant copper-based atacamite. Both the crystalline phase of the inorganic material and the mesoscale structure are directed by the bio-molecules.[2]

Hypothesis. Our central hypothesis from previous annual reports remains unchanged. Namely, we believe that in order to generate intricate biomimetic architectures, matrix mediated nucleation needs to be a multi-step process,[23] This hypothesis is known as "tectonic" nucleation and growth,[24] and we apply our biomimetic interfacially confined peptide to explore this phenomenon at an addressable air-water interface. In this scheme, the final crystalline state is not arrived at via direct epitaxy. Rather, the phase behavior of the organic phase dictates a more complex process, where the kinetics of self-assembly drive the final inorganic morphology. This mesoscale structure is governed by the dynamics of rearrangement of the organic phase not a preformed organic template. In order to understand the pathway-dependent final crystalline structure, we have examined the self-assembly and phase behavior of model peptides confined at interfaces.

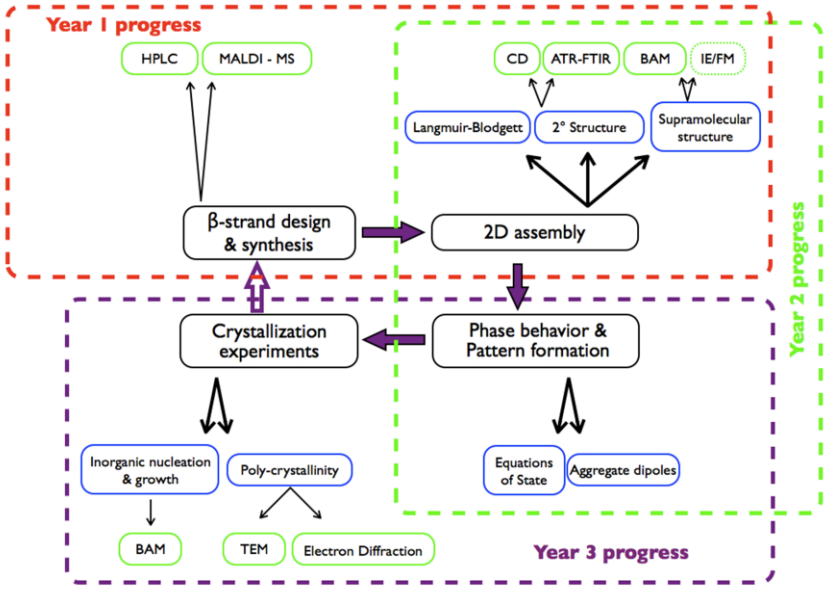

Figure 3. Objectives and progress. Progress in Year 1 (red), Year 2 (green) and Year 3 (purple) are in dashed boxes. We apply a series of interfacial characterization tools (green boxes) to ask fundamental questions about the evolution of complexity in composite materials. The iterative strategy allows us to rationally design control experiment, answering questions regarding the role of self-assembly in materials processing.

The critical transitions between nucleation, growth and, eventually, phase transition can be defined as a series of activation-energy barriers that are controlled by the self-organization of the peptide. The general concept of this behavior is shown in **figure 2**.[23]

To explore this hypothesis, we have developed a set of amphiphilic peptides where we can precisely quantify the thermodynamics of self-assembly and couple the self-assembly process with the dynamics of nucleation and growth. The iterative process for the design and characterization of these peptides as well as our year-by-year objectives are highlighted in **figure 3**. Year one focused on the design, synthesis and assembly of the first and second generation of peptides described below. Year two focused on the structural characterization of the peptides confined at interfaces as well as an analysis of the phase behavior observed. Finally, year three focused on the interfacial crystallization as a function of the peptide's self-assembled state. Our experimental tools that we use to examine both the organic and inorganic phases are highlighted in green, and the year-by-year breakdown of activities is highlighted in the dashed boxes.

Overall, these objectives allow us to quantitatively characterize both self-assembly and nucleation with a set of self-organizing surface-bound peptides. Our methodology imitates nature's processes for making complex hierarchical structures in a parallel fashion, where organic molecules perform two tasks in an integrated fashion. First, the chemical character of the organic molecule templates the nucleation of a particular crystallographic orientation. Second, the nuclei are driven together as the organic molecules self-assemble into higher-order structures. The parallel construction of hierarchical metallic nanostructures requires the application of both processes to integrate the two length scales. If successful, the research can yield fundamental understanding of nucleation in polycrystalline nano-structures as well as applicable systems to template functional hybrid materials.

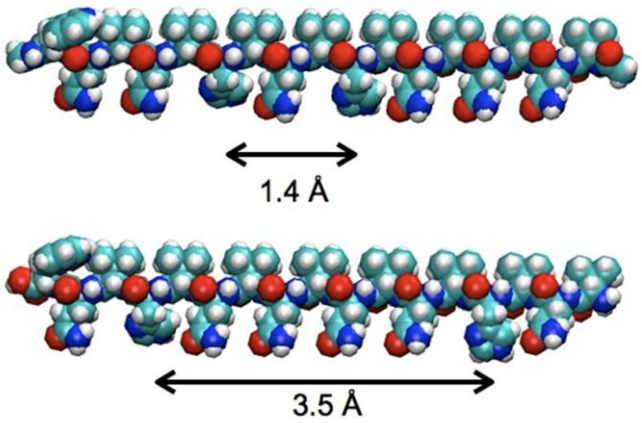

Figure 4. Our third-generation of peptides examines the ability to self-assemble and nucleate an complex metallic structure in a biomimetic fashion. (top) Beta 3H and (bottom) Beta 9H.

2. Findings

This report will describe our findings in three parts: (1) a highlight of germane discoveries made on rational design/synthesis and self-assembly, (2) a set of insights into the phase behavior of the amphiphilic peptide confined at the air-water interface, and (3) a set of results that illustrate how coupled nucleation and self-assembly can lead to complex inorganic nanostructures.

In the design section, we will highlight some minor changes in direction that our findings have compelled us to take. In the assembly and phase behavior section, we will describe several of our major findings regarding the role of sequence periodicity on pattern formation. And, in the crystallization section, we will describe our ongoing collaboration with Hiroshi Matsui at Hunter College to characterize both self-assembly and nucleation and growth pathways to yield an inorganic structure with multiple length scales in gold nanocrystals.

2.1. Rational design and Interfacial assembly

Rational Design. In the previous reports, we describe the rationally design of a set of periodically sequenced peptide designs. Our 'first generation' peptide was a hairpin design that allowed us to examine the role of charge distribution and sequence periodicity on interfacial stability. The peptide behaved as expected, but, in order to precisely pattern the air-water interface and control self-assembly with a simple linear sequence, we developed the next iteration of 17 amino acid peptides. In this report, we focus on the findings from several variants of these sequences, including the role of charge separation and histidine-gold coordination.

We find that these 17 amino acid peptide sequences behave robustly, where periodicity appears to dominate the formation of interfacial self-assembly and structure. If they have a high degree of sheet forming propensity and an alternating hydrophobic-hydrophilic periodicity, then they show consistent phase behavior as a function of surface pressure

The two newest peptide designs are based on splicing *secondary structure-nucleating* and *crystal phase defining* sequences within amphiphilic peptide building blocks. As with previous generations of peptides, there are two canonical rules that take precedent in the *de novo* peptide design algorithms: secondary structure propensity [25] and periodicity.[26,27] Secondary structure propensity refers to the intrinsic inclination of individual amino acids to a given secondary structure, where side-group and steric interactions tend to restrict an amino acid from particular ϕ and ψ conformations.

Periodicity refers to the non-local interactions, where sequence is 'programmed' with a recurring pattern that defines the secondary structure. For instance, to achieve an interfacial β-strand structure, the sequence defining the strand should contain a period of two, meaning that the amino acids at *i* and *i+2* define the hydrophobic face. Because of the chirality of the

amino acids, the side-groups present hydrophobic and hydrophilic residues in and out of the aqueous phase. Moreover, if an amino-acid is periodically repeated in this alternating fashion, then the pattern tends to define one face of a β-strand even if amino-acids that compose the sequence have low sheet-forming propensities.[26] The β-strand surface-active peptide is selected because the structure is stable at the interface and amenable to design. The β-strand structure gives the exceptional control over the spatial distribution of chemical functionality at the interface, where side-chains are presented to the aqueous phase every 0.68 nm (from *i* to *i+2*). Finally, the sheet-like structures have been shown to be stable at interfacial pressures as high as 40 mN/m, prior to collapse.[27,28]

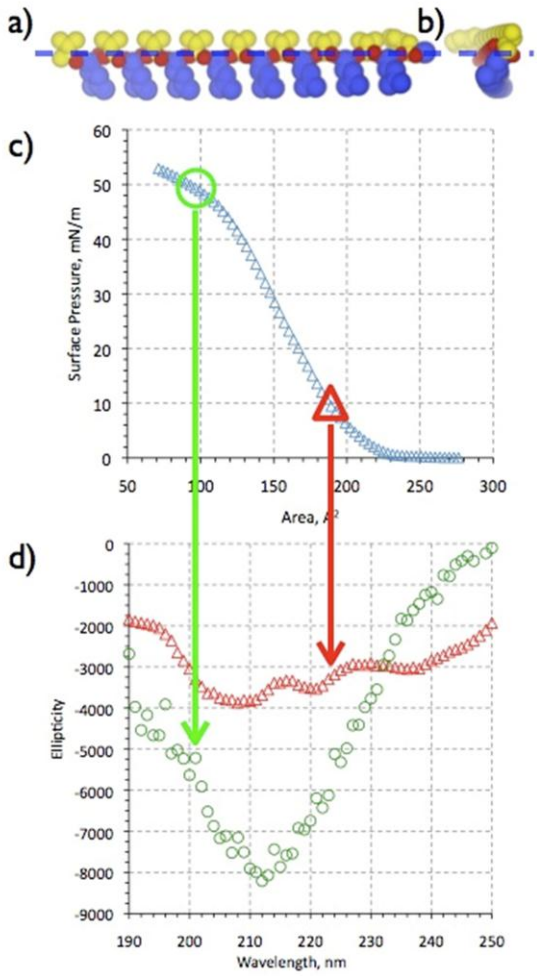

Figure 5. General peptide architecture (a) side view and (b) axial view. (c) Langmuir isotherm. (d) CD of the peptide at low (red) and high (green) surface pressures.

The architecture of the third-generation peptide is shown in **figure 4**. These sequences mimic the Beta 9 and Beta 3 designs from last year's report. Beta 9H and Beta 3H contain the same overall composition, but Beta 3H has two histidines separated by three amino acids (~ 1.4 nm), while Beta 9H has two Histidines separated by 9 amino acids (~ 3.5 nm). These two peptides allow us to investigate the nucleation of inorganic compounds as the peptides self assemble at the interface. Both molecules have similar hydrogen bonding capabilities that would favor self-assembly in the plane of the air-water interface.

Interfacial Assembly. Subsequently, we examine the formation of the self-assembling "templating" structure as we confine the histidine containing peptides at the air-water interface. The peptide molecules are characterized using Langmuir monolayer experiments, Brewster Angle Microscopy, circular dichroism (Figure 5) and Attenuated Total Reflectance Fourier Transform Infrared (ATR-FTIR) spectroscopy. The Langmuir trough confirms the surface activity of the molecules and shows their phase behavior by forcing them from a two-dimensional gaseous to solid phase. Using Brewster Angle Microscopy in conjunction with the Langmuir, we are able to visualize phase behavior as a function of surface pressure. Prior reports described the confirmation of secondary structure using circular dichroism and ATR-FTIR spectroscopy, and the Beta 3H and Beta9H showed similar secondary structure properties at equivalent surface pressures. Therefore, we'll omit the discussion of secondary structure here.

Figure 5 shows the Langmuir isotherms and Brewster Angle Microscopy images for Beta 9H. Brewster Angle microscopy allows us to visualize the phase behavior in the peptide monolayers with the added benefit of not having to use external probes which are needed for other techniques such as fluorescence microscopy[29]. Qualitatively, this behavior is similar to

the behavior of Beta 3H, Beta 9 and Beta 3. A steep liquid condensed region and a liquid expanded to liquid condensed transition occurs at very low surface pressures for all four molecules. In deionized water, both Beta 3 and Beta 9 are negatively charged, while Beta 3H and Beta 9H are neutral. This influence of charge results in much higher phase transition areas for Beta 3 and 9 compared to Beta 3H and 9H. As the surface pressure continues to increase, there is a transition from circular domains to fibrous domains. This transition occurs between 30-50mN/m with fibers being fully formed usually at 50mN/m. Images of the fibers for each of the molecules can be seen in **figure 6**.

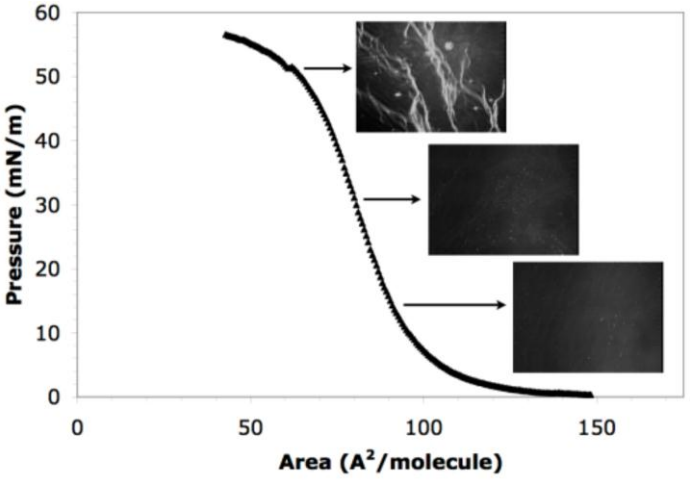

Figure 6. The surface pressure/ area isotherm and Brewster angle microscopy images (width = 220 μm) obtained for Beta 9H at a temperature of 25°C on a deionized water subphase (pH~ 5.5)

2.2. Phase Behavior

We have coupled our analysis of self-assembly thermodynamics using both Brewster Angle Microscope (BAM) and LB isotherms to define the phase behavior as a function of electrostatics. Fitting the Langmuir Isotherms allows us to define thermodynamic characteristics of the self-assembling peptides. Image analysis of the structures resolved with BAM allows us to quantify the intermolecular interactions.

Thermodynamics of self-assembly. To compare the behavior of the glutamic acid-containing and histidine-containing molecules, their pressure/area isotherms have been quantified in terms of an equation of state. Fainerman and coworkers have developed an equation that includes aggregation in two-dimensions at moderate surface pressures[30] and extends this analysis to include interactions between molecules within an aggregate[31,32]. Fainerman's analysis is derived by extending two-dimensional equations of state of gaseous monolayers, known as the Volmer equation, and includes aggregation using the chemical potential for monomers and aggregates, Butler's equation [30]. We apply the following the equation to account for relative instead of absolute surface pressure[33], for example, the relative equation of state for Beta 9H molecule is:

$$P - P_{A=197} = P_{rel} = \left[\frac{RT}{[(A - A_0)(A_C/A)]}\right] - \left[\frac{RT}{[((197 - A_0)(A_C/197)]}\right] \quad (1)$$

The same equation was used for Beta 9, Beta 3H, and Beta 3 except for the reference area.

By fitting the LB data to equation 1, one is able to obtain the parameters A_0 and A_C. A_C as the critical aggregation area, which is analogous to the inverse of the three dimensional critical micelle concentration. This implies that above A_C no aggregates are present, but below A_C large aggregates are present [33]. The term A_0 is described as the limiting molecular area or the area actually occupied by the molecule in the monolayer.

Table 1 has both values for each molecule. Comparing the A_0 values obtained, the histidine containing peptides are smaller than the glutamic acid containing peptides.

Additionally, in both the glutamic acid containing peptides and the histidine containing peptides, the Beta 3 versions are smaller than Beta 9 versions. We also show that the A_C values for the glutamic acid containing peptides are much larger than that of the histidine containing peptides. This result is non-intuitive, indicating that cohesive forces between the glutamic acid containing peptides are greater than the cohesive forces for the histidine containing peptides. However, the cohesive forces in the form of hydrogen bond formation should be similar for each molecule. We believe that the reason the glutamic acid containing molecules aggregate at lower surface concentrations is that the long-range electrostatic repulsion between the molecules forces the molecules to distribute more regularly throughout the interface. On compression, this leads to the local formation of a greater number of smaller aggregates. Additional experiments were conducted with various salt concentrations in the subphase support the hypothesis.

The value of A_C for Beta 3H and Beta 9H are equivalent, indicating that aggregation occurs at the same area for both molecules. However, in the glutamic acid containing peptides, there is a more pronounced difference between the A_C of Beta 3 and Beta 9. Beta 9 has a lower A_C value than Beta 3. Again, at first glance this is counterintuitive; one would expect that Beta 9 peptides possess an A_0 value this is higher than the A_0 of Beta 3, and Beta 9 would subsequently aggregate at a larger area. However, A_C is a measure of cohesive intermolecular forces and not electrostatic repulsion. Therefore, Beta 3 with its centrally localized charge allows for hydrogen bonding with other peptide molecules at the uncharged end of the molecule. This staggered arrangement of peptides could lead to self-assembly at lower interfacial concentrations. In contrast, Beta 9 displays its negative charge is across the entire molecule and thus hydrogen bonding between these molecules would only occur only after the electrostatic repulsion of the entire molecule could be overcome. It is interesting to note that the histidine molecules do not show this A_C trend. We believe that the weaker charge in these molecules makes this effect negligible.

Intermolecular Interactions. To evaluate the Brewster Angle Microscopy images, we use McConnell and coworkers' theory for stripe phases occurring in monolayers[34-36]. Their model balances the free energy contributions of line tension between domains and electrostatic interactions of the domains. They begin with the following equations:

$$F = lp + F_{el} \qquad (2)$$

$$F_{el} = const - \frac{m^2}{2} \oint\oint \frac{1}{r} dl\,dl' \qquad (3)$$

In these equations, F is the free energy, λ is line tension, F_{el} is the electrostatic free energy, and μ is the difference in dipole density between the fluid and the sold phase. By performing the integration in equation 3, one arrives at the following equation defining the formation of the stripe phase:

$$\overline{F_s} = 2m^2 \left(\frac{f}{e_W}\right)\left[\frac{l}{m^2} - \ln\left(\frac{e_W}{2d}\right)\times\frac{\sin(pf)}{pf}\right] \qquad (4)$$

ϕ is the solid area fraction, w is the width of the stripes, and δ is the interdipole distance. If one minimizes this equation with respect to w, one obtains:

$$w = \frac{2dpe}{\sin(pf)} e^{\frac{l}{m^2}} \qquad (5)$$

From our Brewster angle microscopy images, we can obtain values for w and ϕ. These values are obtained by using image analysis software to determine the exact location of the

fibers and calculate both the width of the fibers and the fractional area occupied. The value for δ is obtained by using the molecular area obtained from the Langmuir trough experiments at a pressure of 50 mN/m and then dividing this value by the theoretical length of these molecules, 5.0 nm.

Rearranging equation 5, one obtains equation 6

$$\frac{l}{m^2} = \ln\left(\frac{w\sin(pf)}{2dpfe}\right) \quad (6),$$

which gives the ratio of the line tension over the dipole density. The qualitative behavior for all four peptides is similar, showing that the binary sequence periodicity dominates interfacial self-assembly, but this dimensionless parameter gives us the ability to quantitatively discern the influence of electrostatic on aggregate formation sequences in terms of the forces that are dominating the free energy in our system. Higher values of this number would indicate that line tension between boundaries is higher than electrostatic contributions to the free energy. The values for our four peptides appear in **table 1**.

Table 1 Values of A_0, A_C, and λ/μ^2 for all four peptide molecules and the parameters obtained from the image analysis to find λ/μ^2.

	Beta 9	Beta 3	Beta 9H	Beta 3H
A_0 (Å^2/molecule)	250.24	158.53	74.46	54.93
A_C (Å^2/molecule)	617.61	1121.46	402.14	398.22
w (μm)	0.978	1.129	1.001	0.900
ϕ	0.133	0.172	0.092	0.078
δ(Å)	2.615	2.143	1.289	0.554
λ/μ^2	6.504	6.826	7.258	7.987

When we compare the values obtained, it is evident that the results are in agreement with the Langmuir trough data. The molecules with the greatest electrostatics or smallest λ/μ^2, are the Beta 9 molecules, followed by Beta 3, Beta 9H, and then Beta 3H. When we compare the values of the histidine set to the glutamic acid set, we see that the numbers are larger for the histidine set. Comparing Beta 3 and Beta 9 in both sets of molecules also gives us greater λ/μ^2 numbers for Beta 3 as compared to Beta 9, which again supports the notion that the more localized charge in the Beta 3 molecules allows the peptides to pack more efficiently and would therefore appear to have weaker electrostatics.

Natural systems show an unparalleled ability to assemble composite materials across hierarchical length scales. At the heart of this materials processing phenomenon is the ability to control self-assembly pathways. Our peptides are particularly suited to serve as an organic template capable of rearrangement into particular patterns that define mesoscale structures. We have characterized four simple rationally designed peptide molecules using tools that allow us to quantify the phase behavior and intermolecular interactions. **Table 1** shows a careful thermodynamic analysis for periodically sequenced peptides, resulting in a more lucid understanding of self-assembly under confinement. These tools confirm that all four variations

of our peptide are surface active, form beta sheets at the air-water interface, and form fibrillar domains at high surface concentrations when hydrogen bonding between the molecules dominates the free energy.

2.3. Crystallization Experiments

Recent work on the characterization of crystallization using the third-generation peptide functionalized interfaces has revealed fundamental biomimetic pathways that lead to complexity in metallic structure nucleation. Several experiments were conducted using an inorganic gold precursor. These experiments are executed using a modified protocol from Slocik et al,[37] where a stock solution of metal ions ($HAuCl_4$) is dissolved in the subphase of the Langmuir Blodgett trough. We do not add a reductant to the subphase to initiate the nucleation process. Rather, we allow the tryptophan group on the peptide (see figure 4) at the interface to reduce the gold and initiate formation of metallic structures. After a four-hour incubation period, we observe a red colored film only at the air-water interface while the bulk solution remains clear. In order to characterize the gold structures, we use TEM grids and transfer the interfacial material to the solid substrate by dipping.

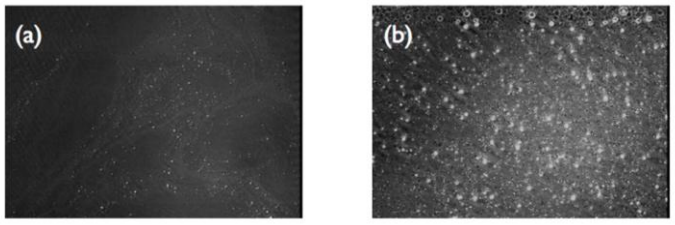

Figure 7. Brewster angle microscopy images taken at a surface pressure of 30mN/m (a) before incubation with Au3+ ions (b) after incubation with Au3+ ions. The width of the images is 220 μm.

Figure 7 shows BAM images of Beta 9H taken at a surface pressure of 30mN/m. The images show the organic template (left) and the air-water interface after incubation with Au^{3+} ions. These images show that there is nucleation occurring at the interface, where the saturated bright spots represents regions where there is a large change in the refractive index. Several experiments are also conducted at surface pressures that are low (10 mN/m) and high (50 mN/m) showing similar BAM results as gold begins to condense. Additional experiments are conducted using TEM and electron diffraction to show the nanoscale structure of the gold as a function of surface pressure and self-assembly.

There is a clear change in the gold structures from TEM images and the diffraction patterns at different surface pressures, **Figure 8**. The images show samples collected at 30mN/m, 40mN/m, and 50mN/m. The image collected at 30mN/m shows an equilateral triangle with sides of approximately 800 nm. The corresponding electron diffraction pattern indicates that the triangle is a single crystal of hexagonal symmetry and can be indexed using the fcc structure of gold. The hexagonal pattern arising in the diffraction indicates that {111} facets bound the crystal[38,39]. The strongest peaks obtained are for the peaks pertaining to the {220} reflections as seen in figure 8a. At 40mN/m figure 8 indicates that the triangular crystal formed is rougher and smaller with sides of approximately 510 nm. The diffraction pattern still has hexagonal symmetry similar to that of the triangle formed at 30mN/m. However, the electron diffraction pattern has small differences to that shown for 30mN/m. There are often multiple diffraction spots in the place of a single diffraction spot, as indicated in the spot that has been circled. Multiple spots suggest that the rougher triangle is made up of multiple single crystals that are formed out of phase. At 50mN/m, we observe that the structure formed is no longer a triangle, but instead a “star-like” figure that has a diameter from point to point of approximately 460 nm. Qualitatively, at these higher pressures, these “star-like” structures appear to be formed from several overlapping triangles. The electron diffraction pattern of this

structure upon close examination still has the hexagonal symmetry found in the other two gold structures. However, the multiple spots effect is more pronounced indicating that the structure is more polycrystalline in nature than the rough triangle.

We have also conducted experiments at surface pressures below 30mN/m, ranging from 5mN/m to 20mN/m. In these experiments, we also observe the formation of triangular structures similar to those formed at 30mN/m in figure 8, but, at surface pressures below 30mN/m, the yield of triangles is lower. We attribute the decrease in yield to be due to the lower number of peptide aggregates present between the pressures of 5-20 mN/m. Since the total amount of peptide at the interface is the same at all surface pressures, we hypothesize that an aggregate of a critical size is necessary for the formation of the single crystal triangle. This phenomena also explains why at higher surface pressures, as is the case for 40mN/m and 50mN/m, the electron diffraction and TEM images indicate the presence of multiple single crystals since the peptide aggregates are much closer together at these higher surface pressures.

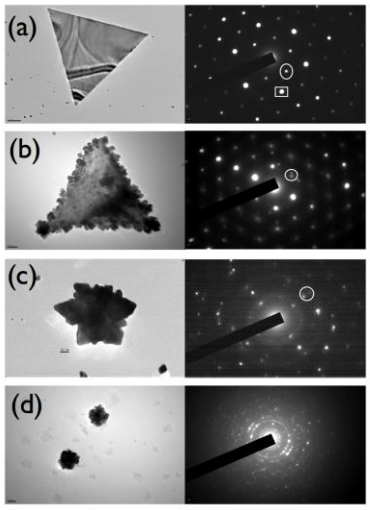

Figure 8. The TEM images and corresponding electron diffraction patterns at varying surface pressures: (a) Beta 9H collected at a surface pressure of 30mN/m, circled diffraction spot corresponds to 1/3 {422}; square:{220} (b) Beta 9H collected at a surface pressure of 40mN/m, circle indicates out of phase diffraction spots (c) Beta 9H collected at surface pressure of 50mN/m, circle indicates multiple out of phase diffraction spots (d) Beta 3 collected at a surface pressure of 30mN/m

The proximity of the peptides changes between 80 $Å^2$/molecule (Π=30 mN/m) and 65 $Å^2$/molecule (Π=50 mN/m) as can be seen in figure 5. We believe that this change in proximity of neighboring peptides causes imidazole groups in the histidine residues of the peptides to buckle at the air/water interface. This leads to multiple single crystals being formed out of phase at the higher surface pressures. Numerous samples obtained from these experiments also show structures related to triangles such as hexagons, truncated triangles, and saw tooth structures. The hexagons and truncated triangles are found in samples obtained from surface pressures of 30mN/m and lower. The size of these structures indicates that the hexagon forms first and, subsequently, growth on three sides of the hexagon are suppressed to form a truncated triangle, and, finally, an equilateral triangle. At pressures greater than 30 mN/m, the saw tooth structure forms and appears to be a series of triangles connected along their vertices. We again hypothesize that this is a result of the proximity of peptide aggregates at higher pressures.

In order to try to understand the formation of these triangular and related structures, two additional experiments are conducted. First, Atomic Force Microscopy (AFM) is applied to determine the thickness of these structures. The AFM measurements are shown in **figure 9**. They indicate that the truncated triangle has a thickness of approximately 20 nm. Therefore, the structures we have been observing are confirmed to platelet structures and not pyramidal. The thinness of these structures is also confirmed using electron diffraction with tilting. In figure 8a, the diffraction pattern corresponding to the triangle formed at 30mN/m shows the forbidden 1/3 {422} reflection. This reflection is only seen in platelet structures in which the surface of the gold is flat[39-42].

Second, a control experiment is conducted at 30mN/m using the Beta 3 peptide that contains no histidine. The TEM images and diffraction patterns for these experiments are shown in figure 8d. Clearly, gold was reduced at the interface. However, the formation of triangular platelets and related structures did not occur. Instead, we observe circular particles with diameters of approximately 100 nm and no preferential growth of any particular plane of gold. This control experiment clearly indicates that the reduction of gold in our system is attributed to the tryptophan residue in both sequences, but that the histidine residue is responsible for providing a directionality of growth and the formation of triangular platelets with the {111} face parallel to the air/water interface. Many metals have facets dominated by the {111} facet, indicating a low energy plane[44]. We suggest that the mechanism of growth of these triangular particles relies on the imidazole side chain binding to the {111} face of gold and inhibiting the growth of that particular plane or, in other words, acting as a capping agent. These fast growing facets will eventually disappear during growth, resulting in a crystal dominated by the slow growing facets[43]. This phenomena of imidazole capping the {111} facet has been observed previously in other imidazole containing molecules such as ionic liquids[41] and C18-imidazole surfactants[44]. In the case of the ionic liquid study, higher concentrations produce plate-like particles similar to those observed at our interfaces, while low concentrations produce polyhedron like particles. This indicated that at lower concentrations, the amount of imidazole containing molecules is not sufficient to inhibit growth of other crystal planes[41].

2. Supported Personnel

The grant funded summer salary for the PI, Raymond Tu. This grant also funded two graduate students: Lina Zhong, who conducted the third generation peptide synthesis, and Lorraine Leon, who conducted all of the characterization experiments described above. Additionally, the grant supported an undergraduate student Phillip Logrippo, who helped Lorraine Leon conduct both the BAM and ATR-FTIR experiments.

3. Collaborations

During the 2010 grant period we did not develop any new collaborations, but we continued to work together with several PIs. We continued to work with **Joel Koplik** from the Levich Institute at CCNY to examine the long-range dynamics of self-assembly of β-strand peptides confined at the air-water interface. Additionally, we are working with **Hiroshi Matsui** from Hunter College, another CUNY college to characterize the inorganic-organic composite material. Finally, we are working with **Jin Montclare** at NYU-Polytechnic to examine bulk phase properties of self-assembling peptides.

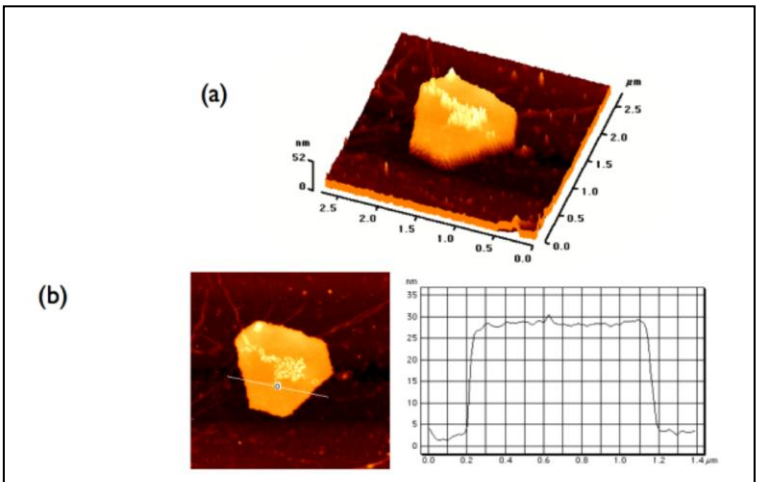

Figure 9. AFM images obtained for a truncated triangle at a surface pressure of 30mN/m (a) Three dimensional image (b) cross section and corresponding thickness profile

4. Publications

During the 2010 grant period we have published two manuscripts: one on the dynamics of peptides at interfaces “Self-Assembly of Rationally Designed Peptides Under 2-D confinement.” Leon, L., LoGrippo, P., Tu, R.S.; Biophysical Journal, 2010, 99, 9. A and one with collaborators on the self-assembly of block polyproteins “Supramolecular assembly and small molecule recognition by genetically engineered protein block polymers composed of two SADs.” Haghpanah, J.S., Yuvienco, C. Roth, E.W., Liang, A. Tu, R.S., Montclare, J.K. Mol. BioSyst., 2010, 6, 1662-1667.

Revisions to a manuscript entitled “Interfacial templating of inorganic nanostructures using a growth directing and reducing peptide” have been sent to Soft Matter. Additionally, a manuscript in in preparation that will focus on the irreversibility of the organic phase during compression and expansion cycles, ”Compression/Expansion hysteresis of β-sheet forming peptides at the air-water interface”.

5. Interactions/Transitions

The focus of our work over the last year has been on examining the fundamental processes that can lead to complex nano-structures in metallic materials. Our key technological transition has been the observation of various gold-nanostructures that are dependent on the surface pressure and, therefore, the self-assembled peptide state. This had led to fundamental contributions in interfacial science, including the understanding intermolecular interactions between self-assembled structures and inorganic nucleation processes. Additionally, we applied these interfaces to understand the fundamental behavior of how natural systems apply nanoscale presentation of organic chemical precursors and cooperative self-assembly processes. We believe that we have access to a new mode of organically controlled materials synthesis, where the non-equilibrium peptide template can direct the formation of inorganic species across multiple length scales.

6. References

(1) Xue, C.; Me traux, G. S.; Millstone, J. E.; Mirkin, C. A. J. Am. Chem. Soc. 2008, 130, 8337.

(2) Lichtenegger, H. C.; Schoberl, T.; Bartl, M. H.; Waite, H.; Stucky, G. D. Science 2002, 298, 389.

(3) Mann, S. Nature 1988, 332, 119.

(4) Mann, S. Biomimetic Materials Chemistry; John Wiley & Sons: New York, NY, 1996.

(5) Aizenberg, J.; Weaver, J. C.; Thanawala, M. S.; Sundar, V. C.; Morse, D. E.; Fratzl, P. Science 2005, 309, 275.

(6) Schaffer, T. E.; IonescuZanetti, C.; Proksch, R.; Fritz, M.; Walters, D. A.; Almqvist, N.; Zaremba, C. M.; Belcher, A. M.; Smith, B. L.; Stucky, G. D.; Morse, D. E.; Hansma, P. K. Chem. Mater. 1997, 9, 1731.

(7) Belcher, A. M.; Wu, X. H.; Christensen, R. J.; Hansma, P. K.; Stucky, G. D.; Morse, D. E. Nature 1996, 381, 56.

(8) Waite, J. H.; Lichtenegger, H. C.; Stucky, G. D.; Hansma, P. Biochemistry 2004, 43, 7653.

(9) Aizenberg, J.; Tkachenko, A.; Weiner, S.; Addadi, L.; Hendler, G. Nature 2001, 412, 819.

(10) Addadi, L.; Weiner, S. Nature 2001, 411, 753.

(11) Kamat, S.; Su, X.; Ballarini, R.; Heuer, A. H. Nature 2000, 405, 1036.

(12) Cha, J. N.; Shimizu, K.; Zhou, Y.; Christiansen, S. C.; Chmelka, B. F.; Stucky, G. D.; Morse, D. E. Proc. Natl. Acad. Sci. U. S. A. 1999, 96, 361.

(13) Landis, W. J. Connective Tissue Research 1996, 35, 1.

(14) Naik, R. R.; Stringer, S. J.; Agarwal, G.; Jones, S. E.; Stone, M. O. Nat. Mater. 2002, 1, 169.

(15) Klaus, T.; Joerger, R.; Olsson, E.; Granqvist, C. G. Proc. Natl. Acad. Sci. U. S. A. 1999, 96, 13611.

(16) Slocik, J. M.; Stone, M. O.; Naik, R. R. Small 2005, 1, 1048.

(17) Sano, K. I.; Sasaki, H.; Shiba, K. Langmuir 2005, 21, 3090.

(18) Nam, K. T.; Kim, D. W.; Yoo, P. J.; Chiang, C. Y.; Meethong, N.; Hammond, P. T.; Chiang, Y. M.; Belcher, A. M. Science 2006, 312, 885.

(19) Meldrum, F. C.; Wade, V. J.; Nimmo, D. L.; Heywood, B. R.; Mann, S. Nature 1991, 349, 684.

(20) Whaley, S. R.; English, D. S.; Hu, E. L.; Barbara, P. F.; Belcher, A. M. Nature 2000, 405, 665.

(21) Ni, J. P.; Lee, S. W.; White, J. M.; Belcher, A. M. Journal of Polymer Science Part B-Polymer Physics 2004, 42, 629.

(22) Lee, S. W.; Mao, C. B.; Flynn, C. E.; Belcher, A. M. Science 2002, 296, 892.

(23) Xu, G. F.; Yao, N.; Aksay, I. A.; Groves, J. T. J. Am. Chem. Soc. 1998, 120, 11977.

(24) Cölfen, H.; Mann, S. Angew. Chem. Int. Ed 2003, 42, 2350.

(25) Chou, P.; Fasman, G. Annu. Rev. Biochem. 1978, 47, 251.

(26) Xiong, H.; Buckwalter, B.; Shieh, H.; Hecht, M. Proc. Natl. Acad. Sci. U. S. A. 1995, 92, 6349.

(27) DeGrado, W.; Lear, J. J. Am. Chem. Soc. 1985, 107, 7684.

(28) Taylor, J. Biochemistry 1990, 29, 5364.

(29) Lheveder, C.; Hénon, S.; Mercier, R.; Tissot, G.; Fournet, P.; Meunier, J. Review of Scientific Instruments 1998, 69, 1446.

(30) Fainerman, V.; Vollhardt, D.; Melzer, V. J. Phys. Chem 1996, 100, 15478.

(31) Fainerman, V.; Vollhardt, D. J. Phys. Chem. B 1999, 103, 145.

(32) Vollhardt, D.; Fainerman, V. B.; Siegel, S. J. Phys. Chem. B 2000, 104, 4115.

(33) Colfer, S.; Kelly, J.; Powers, E. Langmuir 2003, 19, 1312.

(34) McConnell, H. M. Proc Natl Acad Sci USA 1989, 86, 3452.

(35) McConnell, H. M. Annual Reviews in Physical Chemistry 1991, 42, 171.

(36) McConnell, H. M.; Moy, V. T. The Journal of Physical Chemistry 1988, 92, 4520.

(37) Gazit, E.; Nussinov, R. Nanostructure design: methods and protocols; Humana Press: Totowa, 2008; Vol. 474.

(38) Shao, Y.; Jin, Y.; Dong, S. Chemical communications 2004, 2004, 1104.

(39) Sun, Y.; Mayers, B.; Xia, Y. Nano Letters 2003, 3, 675.

(40) Shankar, S.; Rai, A.; Ankamwar, B.; Singh, A.; Ahmad, A.; Sastry, M. Nature Materials 2004, 3, 482.

(41) Zhu, J.; Shen, Y.; Xie, A.; Qiu, L.; Zhang, Q.; Zhang, S. J Phys Chem C 2007, 111, 7629.

(42) Germain, V.; Li, J.; Ingert, D.; Wang, Z.; Pileni, M. J. Phys. Chem. B 2003, 107, 8717.

(43) Yin, Y.; Alivisatos, A. Nature 2004, 437, 664.

(44) Hsu, S.; Hsu, K.; Leong, M.; Lin, I. Dalton Transactions 2008, 2008, 1924.